Annals of Biomedical Engineering, Vol. 38, No. 11, November 2010 *(© 2010)* pp. 3347–3362
DOI: 10.1007/s10439-010-0147-7

Modeling of Hemodialysis Operation

HASAN ERBIL ABACI and SACIDE ALSOY ALTINKAYA

Department of Chemical Engineering, Izmir Institute of Technology, Gulbahce Koyu, 35340 Urla, Izmir, Turkey

(Received 2 November 2009; accepted 17 March 2010; published online 2 September 2010)

Associate Editor Gerald Saidel oversaw the review of this article.

Abstract—In this study, a theoretical model was developed to predict the solute concentrations in patients' blood and optimize the efficiency of the hemodialysis operation. The model takes into account simultaneous mass and momentum transfer on the blood side both in radial and axial directions. A key component of the model is the incorporation of the protein adsorption on the inner surface of the membrane. The validity of the model was confirmed with the experimental data available in the literature for two different types of hemodiafilter. To illustrate the importance of including the radial concentration gradients and protein adsorption kinetics in the model, the experimental data were predicted with and without consideration of these effects. The results have shown that assuming uniform concentration in the radial direction or neglecting protein adsorption on the inner surface of the membrane leads to higher error in predicting the experimental data. In addition, significant error can be introduced in the calculation of the dialysis time if protein adsorption is not considered.

Keywords—Hemodialysis, Protein adsorption, Mass transfer, Momentum transfer, Mathematical model.

NOMENCLATURE

A_s	Membrane surface area (cm^2)
D_∞	Diffusion coefficient in free space of the porous medium (cm^2/s)
$D_{i\mathrm{B}}$	Diffusion coefficient of species i in blood (cm^2/s)
d_{eq}	Equivalent diameter defined by Eq. (30) (cm)
$d_{housing}$	Inner housing diameter of the dialyzer (cm)
J_v	Total volumetric flux (cm/s)
K_o	Overall mass transfer coefficient (cm/s)
K_C	Convective hindrance factor
K_D	Diffusive hindrance factor
K^{IE}	Intercompartmental solute clearance (cm^3/s)
K_t, K_s	Hydrodynamic functions
k_{mD}	Mass transfer coefficient (cm/s)
k	Boltzman constant (cm^2 g/s^2 K)
L	Fiber length (cm)
L_p	Hydraulic permeability (cm/s mmHg)
m_p	Amount of protein adsorbed (g)
N_{fiber}	Number of fibers
N_p	Protein flux toward the membrane surface (g/cm^2 s)
N_i	Mass flux of solute i (g/cm^2 s)
P^*	Pressure (mmHg)
Q	Volumetric flow rate (cm^3/s)
Q_{max1}	Adsorption capacity for primary adsorption (g/cm^2)
Q_{max2}	Adsorption capacity for secondary adsorption (g/cm^2)
r_m	Radius of a protein molecule (cm)
r_s	Radius of a solute (cm)
r_{pore}	Average radius of the pores (cm)
Re	Reynolds' number $\left(\frac{\rho U_{avg} d_{eq}}{\mu}\right)$
R_i	Fiber radius (cm)
r^*	Radial position (cm)
Sc	Schmidt number ($\mu_D/\rho_D D_i$)
Sh	Sherwood number ($k_{mD} d_{eq}/D_\infty$)
T	Temperature (K)
t	Time (s)
U^*	Radial velocity (cm/s)
U_{avg}	Average axial velocity (cm/s)
V	Volume of water (cm^3)
V^*	Axial velocity (cm/s)
$\hat{v}_p$	Specific volume of protein (cm^3/g)
X_p	Thickness of the protein layer (cm)
z^*	Axial position (cm)

Greek letters

ϕ	Partition coefficient
ρ_i	Concentration of species i (g/cm^3)

Address correspondence to Sacide Alsoy Altinkaya, Department of Chemical Engineering, Izmir Institute of Technology, Gulbahce Koyu, 35340 Urla, Izmir, Turkey. Electronic mail: sacidealsoy@iyte.edu.tr

δ	Membrane thickness (cm)
π	Oncotic pressure (mmHg)
μ*	Viscosity (g/cm s)
σ	Length to radius ratio of fiber (L/R_i)
θ	Angular position (cm)
ε	Porosity
λ	The ratio of solute radius to pore radius

Subscripts/superscripts

B	Blood
D	Dialysate
M	Membrane
1	Dense layer of membrane
2	Porous layer of membrane
p	Protein layer
E	Extracellular
I	Intracellular
w	Water
out	Dialysate outlet
UF	Ultrafiltration

INTRODUCTION

Worldwide, over one million patients suffer from chronic renal failure. Most are treated with hemodialysis due to a limited number of donors available for kidney transplants. The efficiency of hemodialysis operation depends on both module design and clinical procedures. The numerous high flux membranes and membrane modules developed to enhance the quality of the treatment need to be tested experimentally before use in clinical applications. This extensive experimentation is usually costly and time consuming. The problem can be overcome by an accurate and reliable mathematical model that can be used as a first pass for evaluating new designs as well as for controlling and optimizing different forms of the therapy.

Numerous efforts have been made to develop theoretical models for predicting the performance of hemodialysis operation. In many of these studies, total solute flux is assumed constant through dialyzer[5,16,17,32,36] and mass transfer of solutes through the membrane is defined with an overall mass transfer coefficient[33,36–38] to include blood, membrane, and dialysate resistances for a given solute. Legallais *et al.*[20] and Raff *et al.*[30] considered the change in both total filtration flux and local transmembrane solute flux through the length of the dialyzer. However, in each study, flow rates, concentrations, and pressures are assumed to be uniformly distributed over the module cross section, and momentum transfer, on both blood and dialysate sides of the membrane are not considered. In a few studies, simultaneous mass and momentum transfers in both radial and axial directions through the dialyzer are taken into account.[26,28] Noda and Gryte[28] expressed the fluid velocity through the inside of a hollow fiber by that of the parabolic Poiseuille flow, while the velocity profile for the flow through the outside of the fiber was obtained from the literature. In their model, it is assumed that the shape of the cross-sectional concentration profile is constant throughout the major part of the dialyzer. As a result, the solute flux across the membrane becomes spatially constant, the sum of the volumetric flow rates of the fluids in each region becomes zero, and the axial bulk concentration gradients through the blood and dialysate sides become constant and identical to each other. Moussy[26] also considered simultaneous mass and momentum transfers in each region of the hollow fiber dialyzer. In the lumen section of the hollow fiber, velocity profiles and pressure were described in terms of existing analytic expressions. For flow through the shell side, the analytic expressions for the radial and axial velocity profiles and pressure distribution were derived based on a similarity solution. The axial variation in lumen pressure, shell pressure, and osmotic pressure were also taken into account. Even though the models of Noda and Gryte[28] and Moussy[26] take into account the momentum and mass transfers, they neglect the accumulation of rejected large molecules on the inner surface of the membrane. Elution profiles obtained experimentally from the used dialyzers showed that hemodialysis membranes adsorb a lot of proteins.[10] Thus, consideration of the kinetics of protein adsorption is an important issue for the accuracy of the mathematical model.

In this study, a theoretical model was developed to predict the *in vitro* performance of commercial hemodialysis units. The model takes into account simultaneous momentum and mass transfers on the blood side both in radial and axial directions. Mass transfer is assumed to take place both by diffusion and convection in the radial direction, while convection is considered to be the dominant mass transfer mechanism in the axial direction. Furthermore, adsorption of rejected, large blood molecules on the inner surface of the membrane is taken into account. Model predictions were validated with the clearance measurements for different model solutes obtained at different net ultrafiltration rates and blood flowrates as well as with the inlet and outlet pressure measurements in blood and dialysate compartment of the dialyzer. The importance of including radial concentration gradient and protein adsorption kinetics in the model was assessed by predicting the experimental clearance data with and without consideration of these effects. The clearance predictions were also compared with those obtained from another mathematical model existing in

the literature. Simulations were performed for different cases to illustrate the power of the model and wealth of information that cannot be obtained otherwise.

THEORY

Whole Body Clearance Model

In order to observe the effects of model parameters, most importantly, the effect of protein adsorption on the efficiency of the hemodialysis process, evaluating the concentration values in the patients' blood is more appropriate than evaluating the concentrations at the dialyzer outlet for a given inlet concentration. Therefore, mass balance calculations of solutes are necessary accounting for the total body water. In the model, solute transfer between blood vessels and interstitial fluid is assumed to be very fast so that mass transfer kinetics inside the body can be considered to occur only between two main compartments: the intracellular compartment (2/3 of total water volume), and the extracellular compartment (1/3 of total water volume).[23] As schematically represented (Fig. 1), blood is circulated between the hemodialyzer and the extracellular compartment, while the intracellular water is being cleaned by the mass transfer between the two compartments.

Assuming that there is perfect mixing in both compartments, a mass balance of each solute, i, in the extracellular water yields:

$$\frac{d(V^{\mathrm{E}}\rho_i^{\mathrm{E}})}{dt} = (Q_{\mathrm{B}} - Q_{\mathrm{UF}})\rho_i^{\mathrm{out}} - Q_{\mathrm{B}}\rho_i^{\mathrm{E}} + K_i^{\mathrm{IE}}(\rho_i^{\mathrm{I}} - \rho_i^{\mathrm{E}}) \tag{1}$$

The change of each solute concentration in the intracellular water is given as

$$\frac{d(V^{\mathrm{I}}\rho_i^{\mathrm{I}})}{dt} = -K_i^{\mathrm{IE}}(\rho_i^{\mathrm{I}} - \rho_i^{\mathrm{E}}) \tag{2}$$

Equations (1) and (2) are coupled with the model equations derived in the next section for solute transport through the dialyzer. Such a coupling is required since the inlet concentration for the extracellular compartment, ρ_i^{out}, is the solute concentration at the exit of the dialyzer. In the following sections, model equations through the dialyzer will be derived.

Dialyzer Model

Geometry and Assumptions

A typical hollow fiber geometry used for a hemodialysis operation is illustrated in Fig. 2. In this configuration, blood and synthetic dialysate solution flow counter currently through the inside of hollow fibers and outside of the fiber walls made from dialysis membranes, respectively. The membrane is assumed to have an asymmetric structure with a very thin dense skin layer (δ_1) supported by a thick porous layer (δ_2). Small toxic compounds such as urea and low molecular weight proteins can permeate through the membrane; on the other hand, proteins with a molecular weight greater than 60 kDa are rejected, which then accumulate on the surface of the membrane. Thus, the thickness of the adsorbed protein layer, $X_{\mathrm{p}}(t)$, changes with time during hemodialysis operation.

Model equations derived here are general in nature and described by the following assumptions and restrictions:

1. The dialysis operation runs at pseudo-steady state since protein adsorption at the membrane surface is assumed to take place rapidly at each time interval.
2. There is symmetry in the dialyzer, and the angular velocity is zero. Axial and radial velocities change both in axial and radial directions.
3. The blood is a binary solution consisting of a small solute or low molecular weight protein

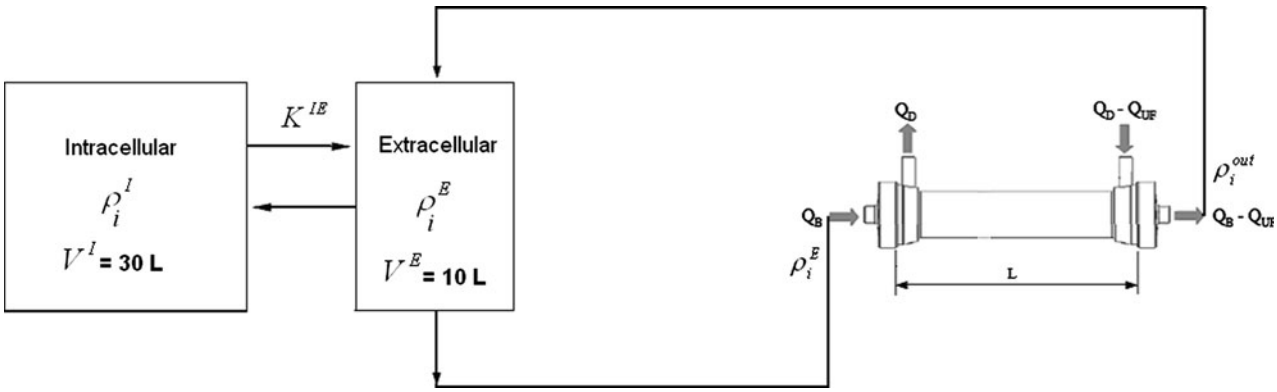

FIGURE 1. Schematic diagram of two compartment whole body clearance model.

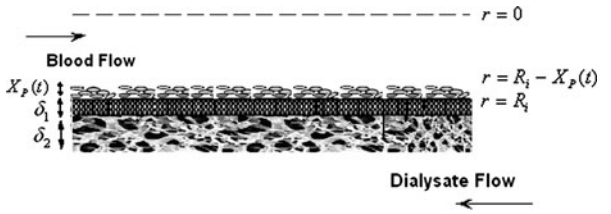

FIGURE 2. Schematic representation of model geometry.

which can permeate through the membrane and a large molecular weight protein (>60 kDa) rejected by the membrane.

4. Solute concentration changes both in axial and radial directions.
5. The partial specific volumes of the solutes in the blood are independent of concentration and equal to each other so that the density of the mixture remains constant.
6. The shear rates in the hollow fibers and outside of the fibers are low; thus, the blood and dialysate solutions are considered Newtonian fluids.
7. Adsorbed protein molecules form an additional uniformly packed porous layer on the membrane surface.
8. There are no homogeneous reactions in the blood or in the dialysate solution.
9. The diffusion coefficients of the solutes in the blood are independent of concentration.
10. Solute transfer on the dialysate side can be expressed with an empirical equation.
11. The very small aspect ratio of the fibers ($\sigma = R_i/L$) associated with a low Reynolds number produces $R_e\sigma \ll 1$, and makes it possible to use the lubrication approximation.[19]
12. The dominant mass transfer mechanism in the axial direction is convection, i.e., axial diffusion is assumed to be negligible.

To facilitate solution, the model equations were written in terms of dimensionless variables. In the following sections, dimensionless forms of the equations will be presented. All of the variables used in the equations, both in dimensional and dimensionless forms, are listed in Table 1.

Total Continuity and Conservation of Momentum Equations

The total continuity equation can be expressed as follows utilizing the first, second, and fifth assumptions listed above:

$$\frac{\partial V}{\partial r} + \frac{V}{r} + \frac{\partial U}{\partial z} = 0 \tag{3}$$

TABLE 1. Dimensional and dimensionless forms of the variables used in model equations.

Model variables	
Dimensional forms	Dimensionless forms
r^*	$r = \frac{r^*}{R_i}$
z^*	$z = \frac{z^*}{L}$
U^*	$U = \frac{U^*}{U_{avg}}$
V^*	$V = \frac{V^* L}{U_{avg} R_i}$
P^*	$P = \frac{P^* R_i^2}{L\mu_w^* U_{avg}}$
$\mu_B{}^*$	$\mu = \frac{\mu_B^*}{\mu_w^*}$

Based on the lubrication approximation and the first, second, fifth, and sixth assumptions, r, θ, and z components of the Navier–Stokes equations are described below:

$$\frac{\partial P}{\partial r} = 0 \quad \frac{\partial P}{\partial \theta} = 0 \tag{4}$$

$$\frac{\partial P}{\partial z} = \frac{1}{r}\frac{\partial}{\partial r}\left[r\mu\frac{\partial U}{\partial r}\right] \tag{5}$$

From Eqs. (4) and (5), the axial velocity is given by the following expression[24]:

$$U = \frac{\int_r^1 \frac{r'}{\mu} dr'}{\int_0^1 \frac{r^3}{\mu} dr} \tag{6}$$

The radial velocity is obtained from the integration of the overall continuity equation:

$$V = -\frac{1}{r}\int_0^r r' \frac{\partial U}{\partial z} dr' \tag{7}$$

It is evident from Eq. (6) that if the viscosity of the blood is assumed to be constant, then the axial velocity is no longer a function of the axial position and the radial velocity becomes zero. However, this assumption is not valid since the proteins in blood increase the viscosity of plasma to a value that is 98% higher than that of water.[35] We have used the relation proposed by Pallone and Petersen[29] to describe the change in the dimensionless blood viscosity with respect to the plasma protein concentration:

$$\mu = 1 + \left(\frac{\mu_{pR}}{\mu_w^*} - 1\right)\frac{\rho_p^B}{C_{pR}} \tag{8}$$

where $\mu_{pR} = 1.22 \times 10^{-3}$ Pa s; $C_{pR} = 70$ g/L. In this relationship, Fahreus effect and redistribution of ions as a result of Donnan equilibrium are neglected.

Protein Adsorption Model

In our model, we have assumed that large protein molecules which cannot diffuse into the membrane pores adsorb on the surface. In addition, it is assumed that adsorption is irreversible, multilayer type, and adsorbed protein molecules form a uniform packing. The irreversible primary and secondary adsorption mechanisms can be described by the following reactions:

$$S + P \rightarrow P_{\text{ads}} \cdot S \quad \text{(primary adsorption)} \tag{9}$$

$$P_{\text{ads}} + P \rightarrow P_{\text{ads}} \cdot P_{\text{ads}} \quad \text{(secondary adsorption)} \tag{10}$$

Considering the primary and secondary adsorption rates, the change in the total amount of proteins adsorbed with time can be written as follows:

$$\frac{dm_{\text{P}}}{dt} = \frac{dm_{\text{P1}}}{dt} + \frac{dm_{\text{P2}}}{dt} \tag{11}$$

The rates of both primary and secondary adsorption are expected to be high at the early stages of the process. Then, they become slower and reach the equilibrium capacity. The secondary adsorption begins after primary adsorption, and it is assumed to speed up as the amount of adsorbed proteins during primary adsorption increases. According to these restrictions, the rates of primary and secondary adsorption are expressed by the following equations in the manner similar to that described by Nakamura and Matsumoto[27]:

$$\frac{dm_{\text{p1}}}{dt} = N_{\text{p}}^{\text{B}} A_{\text{s}} \left(1 - \frac{m_{\text{p1}}}{Q_{\max 1} A_{\text{s}}}\right) \tag{12}$$

$$\frac{dm_{\text{p2}}}{dt} = N_{\text{p}}^{\text{B}} A_{\text{s}} \left(\frac{m_{\text{p1}}}{Q_{\max 1} A_{\text{s}}}\right)\left(1 - \frac{m_{\text{p2}}}{Q_{\max 2} A_{\text{s}}}\right) \tag{13}$$

In terms of protein layer thickness, total amount of adsorbed proteins, m_{p}, can be expressed as

$$m_{\text{p}} = \pi L \left(2R_i X_{\text{p}} - X_{\text{p}}^2\right) \rho_{\text{ads.layer}} \tag{14}$$

where the density of the adsorbed protein layer, $\rho_{\text{ads.layer}}$, is calculated as

$$\rho_{\text{ads.layer}} = \left(1 - \varepsilon_{\text{p}}\right) \frac{1}{\hat{v}_{\text{p}}} \tag{15}$$

The porosity of the adsorbed protein layer (ε_{p}) is taken as 0.477 since the protein molecules are assumed to form a regular packing on the surface.[34] Utilizing Eqs. (11) through (15), the change in the protein layer thickness with time is described below:

$$\frac{dX_{\text{p}}}{dt} = \frac{N_{\text{p}}^{\text{B}} \hat{v}_{\text{p}}}{\left(1 - \varepsilon_{\text{p}}\right)} \left[1 - \left(\frac{m_{\text{p1}}}{Q_{\max 1} A_{\text{s}}}\right)\left(\frac{m_{\text{p2}}}{Q_{\max 2} A_{\text{s}}}\right)\right] \tag{16}$$

The total protein flux toward the membrane surface is described in terms of convective and diffusive mass transfer mechanisms:

$$N_{\text{p}}^{\text{B}} = V^* \rho_{\text{p}}^{\text{B}} \Big|_{r^* = R_i - X_{\text{p}}} - D_{\text{pB}} \frac{\partial \rho_{\text{p}}^{\text{B}}}{\partial r^*} \Big|_{r^* = R_i - X_{\text{p}}} \tag{17}$$

Species Continuity Equation

A dimensionless species continuity equation for the toxic solute in the blood can be written as follows by using the assumptions 1, 2, 3, 4, 5, 8, 9, and 12:

$$V \frac{\partial \rho_i^{\text{B}}}{\partial r} + U \frac{\partial \rho_i^{\text{B}}}{\partial z} = \frac{1}{Pe} \left[\frac{\partial^2 \rho_i^{\text{B}}}{\partial r^2} + \frac{1}{r} \frac{\partial \rho_i^{\text{B}}}{\partial r}\right] \tag{18}$$

where $Pe = U_{\text{avg}} R_i^2 / D_{i\text{B}} L$ is the dimensionless Peclet number which is defined as the ratio of convective to diffusive mass transfer where $U_{\text{avg}} = Q_{\text{B}} / 2\Pi R_i L$. It is evident from Eqs. (4) and (18) that even though the pressure change in the radial direction becomes negligible with the lubrication approximation, all radial velocity terms persist in the species continuity equation for the solute in the blood.

Solute concentrations at the dialyzer inlet are taken as the solute concentrations in the patients' blood and updated at each time step. It is assumed that is there is symmetry around the centerline of the fibers for the solute concentration. Also, the solute flux is no longer assumed to be continuous at the blood–membrane interface due to deposition of proteins on the membrane surface. Hence, following boundary conditions are used in the solution of Eq. (18):

$$z^* = 0, \quad 0 \le r^* \le R_i - X_{\text{p}}(t) \rightarrow \rho_i^{\text{B}} = \rho_i^{\text{E}}(t) \tag{19}$$

$$0 \le z^* \le L, \quad r^* = 0 \rightarrow V = 0, \quad \text{and} \quad \frac{\partial \rho_i^{\text{B}}}{\partial r} = 0 \tag{20}$$

$$0 \le z^* \le L, \quad r^* = R_i - X_{\text{p}}(t) \rightarrow (N_i)^{\text{B}} - N_i^{\text{P}} \frac{R_i}{R_i - X_{\text{p}}(t)} = \frac{dX_{\text{p}}}{dt} \left(\rho_i^{\text{B}} - \rho_i^{\text{P}}\right) \tag{21}$$

Equation (21) was derived from a jump mass balance written for the solute. The term on the right-hand side of Eq. (21) stands for the rate of protein layer thickness change with respect to time and is obtained from Eq. (16). In addition, the solute flux through a porous protein layer, N_i^{P}, can be described due to both diffusion and convection[8]:

$$N_i^{\text{P}} = K_{\text{CP}} J_{\text{v}} \rho_i^{\text{P}} - \varepsilon_{\text{P}} K_{\text{DP}} D_{\infty} \frac{d\rho_i^{\text{P}}}{dr} \tag{22}$$

Previously, Morti *et al.*[25] derived an explicit expression for solute flux through a two-layered membrane under

steady-state conditions. In this study, this expression has been extended for a three-layered case in which layer 1 corresponds to porous protein layer, while layers 2 and 3 represent dense and porous regions of the asymmetric membrane, respectively. To derive the new expression, Eq. (22) was integrated over the thickness of each layer, and the solute concentrations at the blood–protein and the membrane–dialysate interfaces were expressed in terms of the external solute concentrations using equilibrium partition coefficients.

$$\phi_1 = \frac{\rho_i^{\mathrm{P}}|_{r^*=R_i-X_{\mathrm{p}}(t)}}{\rho_i^{\mathrm{B}}|_{r^*=R_i-X_{\mathrm{p}}(t)}}, \quad \phi_2 = \frac{\rho_i^{\mathrm{M}}|_{r^*=R_i+\delta}}{\rho_i^{\mathrm{D}}|_{r^*=R_i+\delta}},$$
$$\text{and} \quad \phi_{\mathrm{P}} = \frac{\rho_i^{\mathrm{P}}|_{r^*=R_i}}{\rho_i^{\mathrm{M}}|_{r^*=R_i}} \tag{23}$$

Then, the following equation was obtained for the solute flux through the adsorbed protein layer and each region of the membrane:

$$N_i^{\mathrm{P}} = N_i^{\mathrm{M}} = \frac{\left[\exp(A+B+C)\frac{\rho_i^{\mathrm{B}}}{\phi_{\mathrm{p}}} - \rho_i^{\mathrm{D}}\right] K_{\mathrm{C2}} J_{\mathrm{v}}}{\exp(B)\left[\exp(A)\left[\frac{K_{\mathrm{C2}}}{K_{\mathrm{C1}}} + \exp(C)\frac{K_{\mathrm{C2}}}{\phi_{\mathrm{p}} K_{\mathrm{CP}}} - \frac{K_{\mathrm{C2}}}{\phi_{\mathrm{p}} K_{\mathrm{CP}}}\right] - \frac{K_{\mathrm{C2}}}{K_{\mathrm{C1}}} - \exp(-B) + 1\right]} \tag{24}$$

where

$$A = \frac{\delta_1 K_{\mathrm{C1}} J_{\mathrm{v}}}{\varepsilon_1 K_{\mathrm{D1}} D_\infty}, \quad B = \frac{\delta_2 K_{\mathrm{C2}} J_{\mathrm{v}}}{\varepsilon_2 K_{\mathrm{D2}} D_\infty}, \quad \text{and} \quad C = \frac{X_{\mathrm{p}} K_{\mathrm{CP}} J_{\mathrm{v}}}{\varepsilon_{\mathrm{p}} K_{\mathrm{DP}} D_\infty} \tag{25}$$

Total volumetric flux, J_{v}, in Eqs. (22) and (24) depends on the pressure difference between blood and dialysate compartments and the hydraulic permeability, as described below:

$$J_{\mathrm{v}} = L_{\mathrm{P}}\left[P_{\mathrm{B}}^* - P_{\mathrm{D}}^* - \pi(z)\right] \tag{26}$$

In Eq. (26), blood pressure is calculated from Eq. (5) and oncotic pressure, $\pi(z)$ is expressed in terms of the total protein concentration in blood[18]:

$$\pi(z) = 0.21\rho_{\mathrm{p}}^{\mathrm{B}}(z) + 1.6\times10^{-3}\rho_{\mathrm{p}}^{\mathrm{B}}(z)^2 + 9\times10^{-6}\rho_{\mathrm{p}}^{\mathrm{B}}(z)^3 \tag{27}$$

where $\rho_{\mathrm{p}}^{\mathrm{B}}$ is in g/L, and π is in mmHg. The pressure on the dialysate side, P_{D}^*, is dependent on the geometry of the module and the configuration of the fibers. The change in dialysate pressure with axial position is expressed with a modified form of the Hagen–Poiseuille equation[13]:

$$\frac{dP_{\mathrm{D}}^*}{dz} = \frac{-32\mu_{\mathrm{D}}^*}{S_{\mathrm{eq}}(d_{\mathrm{eq}})^2} Q_{\mathrm{D}} \tag{28}$$

where S_{eq} and d_{eq} are defined as

$$S_{\mathrm{eq}} = \frac{\pi d_{\mathrm{housing}}}{4} - N_{\mathrm{Fiber}}\pi(R_i - X_{\mathrm{p}} + \delta_1 + \delta_2) \tag{29}$$

$$d_{\mathrm{eq}} = \frac{4S_{\mathrm{eq}}}{\left(2N_{\mathrm{Fiber}}\pi(R_i - X_{\mathrm{p}} + \delta_1 + \delta_2) + \pi d_{\mathrm{housing}}\right)} \tag{30}$$

Net ultrafiltration rate Q_{UF} can be defined as the integration of total volumetric flux, J_{v}, along the fiber length and given as

$$Q_{\mathrm{UF}} = \int_{z^*=0}^{z^*=L} J_{\mathrm{v}}(z^*)\cdot 2\pi\cdot r^* dz^* \tag{31}$$

Q_{UF} is not used as a direct input parameter in the model equations to estimate the solute clearance of dialyzer; instead it is calculated according to the blood pressure inputs. In order to see the effect of this parameter on the solute clearances, blood pressure inputs are changed to give the desired Q_{UF} values for the simulations.

The solute transfer on dialysate side is defined by an empirical equation as follows:

$$N_i = k_{\mathrm{mD}}\left(\rho_i^{\mathrm{D}}|_{r^*=R_i+\delta} - \rho_i^{\mathrm{D,Bulk}}\right) \tag{32}$$

where k_{mD} is the mass transfer coefficient of solute i, in the dialysate compartment. The effects of fiber configuration and packing density of the fibers on the mass transfer of solutes were taken into account with the mass transfer coefficient of solutes in the dialysate solution as will be shown in the next section.

DETERMINATION OF MODEL PARAMETERS

The structural properties of the membrane such as porosity, hydraulic permeability, and pore size were acquired from the literature for different types of membranes.

The diffusive and convective hindrance factors, K_{D} and K_{C}, were calculated from the analytic expressions derived by Bungay and Brenner[3] for rigid spherical solutes in uniform cylindrical pores.

$$K_{\mathrm{D}} = \frac{6\pi}{K_{\mathrm{t}}} \tag{33}$$

and

$$K_C = \frac{(2-\phi)K_s}{2K_t} \tag{34}$$

The equilibrium partition coefficient, ϕ, was estimated from Eq. (35)

$$\phi = (1-\lambda)^2 \quad \lambda = \frac{r_s}{r_{pore}} \tag{35}$$

which was also derived for spherical solutes in a cylindrical pore.[12] The procedure for calculating the hydrodynamic functions K_t and K_s can be found elsewhere.[3]

The pore size of the adsorbed protein layer was assumed to be equal to the radius of a circle that has the same area as the pore between regularly packed molecules. Thus, it was estimated from the following equation:

$$r_{pore} = r_m\sqrt{\frac{4}{\pi}-1} \cong 0.523 r_m \tag{36}$$

In protein adsorption calculations, bovine serum albumin was used as the model protein; therefore, the radius of the adsorbed protein molecule, r_m, was taken as 29.7×10^{-10} m^3. The mass transfer coefficient of the solute on the dialysate side was estimated from an expression derived by Dahuron and Cussler.[7]

$$Sh = \frac{k_{mD}d_{eq}}{D_\infty} = 8.8\left(\frac{d_{eq}}{L}\right)ReSc^{0.33} \quad Re = \frac{\rho U_{avg}d_{eq}}{\mu} \tag{37}$$

TABLE 2. Input parameters used in the simulations.

Parameter	Value
V^E (mL)	13.3[6]
V^I (mL)	26.7[6]
μ_w^* (g/cm/s)	0.00692[15]
Q_{UF} (cm^3/s)	0[16]
$\hat{v}_p$ (cm^3/g)	0.734[4]
Q^a_{max1} (g/cm^2)	11.7×10^{-6}
Q^a_{max2} (g/cm^2)	5.87×10^{-6}
K^{IE} (mL/min)	
Urea	600[6]
Creatinine	275[6]
Vitamin B12	125[6]
Inulin	90[6]
Myoglobin	40[6]
r_s (Å)	
Urea	1.5[14]
Creatinine[b]	3.7
Vitamin B12[c]	6.5
Inulin	14.8[31]
Myoglobin	19.3[11]

[a]Measured in our laboratory.
[b]Calculated from Stokes–Einstein equation, Eq. (38), using reported diffusivity value of creatinine of 9.63×10^{-6} cm^2/s.[30]
[c]Calculated from Stokes–Einstein equation, Eq. (38), using reported diffusivity value of vitamin B12 of 4.1×10^{-6} cm^2/s.[9]

The diffusivity of solutes in blood was estimated from Stokes–Einstein's equation[22]:

$$D = kT/(6\pi\mu_B^* r_s) \tag{38}$$

where viscosity of blood, μ_B^*, was estimated from Eq. (8) and the radii of the solutes, r_s, are listed in Table 2.

SOLUTION OF THE MODEL EQUATIONS

Model equations shown in the previous section are coupled nonlinear, partial, and ordinary differential equations. To facilitate the numerical solution, all equations were put into dimensionless forms. In addition, a coordinate transformation was applied to compensate for the moving boundary that occurs due to accumulation of the proteins on the inner surface of the membrane. The differential equations were converted into algebraic forms by discretizing them with the finite difference approximation. The integrals given in Eqs. (6) and (7) for axial and radial velocities were first transformed into Trapezoidal numerical integration form and then involved into general finite difference equations. Finally, the nonlinear algebraic equations were solved simultaneously in MATLAB 7 using the Levenberg–Marquardt method.

Based on our assumptions, time step for the estimation of protein thickness was determined to be the space time of blood in the dialyzer, $\Delta t = L/U_{avg}$. At each time step, protein thickness was updated and then used for the estimation of solute concentrations in equilibrium with the new protein layer thickness as described above. Simulations were run using AMD Turion 2.3 GHz processor and simulation time is approximately 3.0 s per each time step and 9.8 min to estimate the solute concentrations in patient's blood after 1 h of hemodialysis. The details of the numerical solution algorithm can be found in the thesis of Abaci.[1]

RESULTS AND DISCUSSION

Model Validation

The accuracy of our model predictions was tested by comparison with two sets of experimental data available in the literature. The first set of experimental data was collected by Jaffrin *et al.*[16] for the clearances of creatinine, vitamin B12, and myoglobin. Experiments were performed with saline instead of blood by using a Hospal Filtral 12 AN69HF type hemodiafilter at a fixed dialysate flowrate of 500 mL/min and at different net ultrafiltration rates. Outlet concentrations of each solute were measured collecting three samples from the dialyzer outlet, and all error values were found to be

TABLE 3. Structural properties of the Hospal Filtral 12 AN69HF type hemodiafilter.[20]

	Effective length (cm)	Fiber radius (μm)	Number of fibers	Inner housing diameter (cm)	Thickness (μm)
Hospal Filtral 12 AN69HF type hemodialyzer	20	110	8500	3.9	45

	Membrane area (m^2)	Porosity	Pore size (Å)	Fraction of dense layer	Hydraulic permeability (cm/s mmHg)
Hospal Filtral 12 AN69HF type hemodialyzer	1.15	0.8	17.8	0	7.5×10^{-7}

less than 1% mean. The structural properties of the dialyzer used in the simulations are given in Table 3. Figure 3 shows that model predictions compare well with the experimental data. The model slightly underestimates the data in the case of myoglobin. This can be attributed to uncertainties in the estimation of its diffusion coefficient from the Stokes–Einstein equation, which is usually only valid for low molecular weight solutes. The maximum deviation in the predicted values of myoglobin clearance was found to be 11%. Experimental data and model predictions indicate that increasing blood flow rate from 100 to 500 mL/min enhances the clearance of creatinine by a factor of almost 6, while it has almost no influence on the clearance of large solute myoglobin. The enhancement in the clearance of creatinine with increasing blood flow rate can be attributed to an increase in the volumetric flux through the dialyzer. On the other hand, the clearance of large molecules such as myoglobin is not influenced by the enhancement of the volumetric flux since it is mainly controlled by its transport through the membrane. This is supported by comparing the change in the overall mass transfer coefficient $\times$ area of the solutes ($K_o \times A_s$) with respect to blood flowrate calculated from the expression used in the study of Leypoldt *et al.*[21] It was found that, when the blood flow rate values are increased from 100 to 400 mL/min, $K_o \times A_s$ of creatinine increases from 179 to 298 cm^3/s, whereas that of myoglobin shows a relatively inconsiderable increase from 22.8 to 23.1 cm^3/s consistent with the predictions shown in Fig. 3. The reciprocal of the overall mass transfer coefficient is the overall resistance to mass transfer which is made up of three additive contributions from the blood and dialysate boundary layers and the membrane. Thus, the insignificant change in the myoglobin overall mass transfer coefficient is an indication that its clearance from the blood is mainly controlled by the membrane. The influence of the blood flow rate on the clearance of the small molecular weight solutes diminishes at high flow rates, since the resistance of the blood side to the mass transfer of the solutes becomes negligibly small which is in agreement with the experimental results reported by Leypoldt

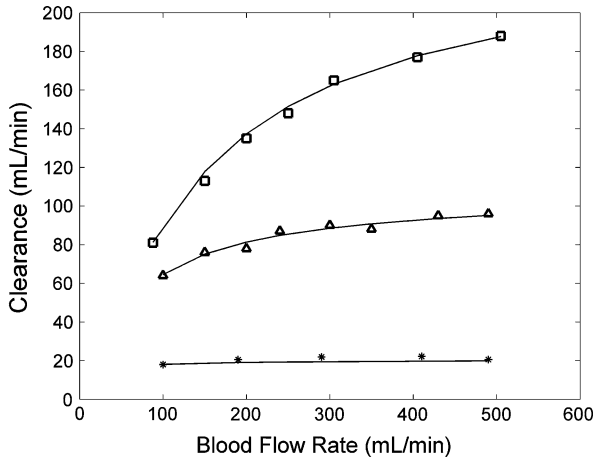

FIGURE 3. Comparison of model results with the experimental data[16] for the clearances of molecules; (□) Creatinine, (△) Vit. B12, and (◆) Myoglobin. Q_D = 500 mL/min, Q_{UF} = 0 mL/min.

et al.[21] The experimental data collected by Jaffrin *et al.*[16] have also been used by other researchers to test the validity of their model predictions. Legallais *et al.*[20] compared the predictive ability of four different models with their own model for clearance enhancement of the solutes as a function of the net overall filtration flow rate. Based on sum of squared residuals (SSR) values, they have concluded that their model predicts the clearance enhancements in closer agreement than the other models proposed in the literature. Owing to best performance of Legallais *et al.*'s model among others, we have compared the predictive ability of our model only with that model and the results are shown in Tables 4, 5, and 6 according to the structural properties of Hospal Filtral 12 AN69 dialyzer given in Table 3. The difference between the experimental and predicted clearance enhancements of creatinine by both models is close to each other. On the other hand, our model yields more accurate predictions for the clearance enhancements of Vitamin B12 and myoglobin. It should be emphasized that our model is completely predictive and does not require any fitting parameter; however, in the model of Legallais *et al.*,[20] diffusive permeabilities of the solutes should be known

TABLE 4. Comparison of experimental data[16] with the predictions obtained from Legallais *et al.*'s model[20] and the model in this article for the enhancement of creatinine clearance.

Q_F (mL/min)	Clearance enhancement[a] Experimental	Legallais *et al.*[20]	This article
20	0.0513	0.053	0.0531
40	0.1245	0.107	0.1069
60	0.1866	0.160	0.1583
SSR		1.0×10^{-3}	1.1×10^{-3}

Data were collected using saline in substitution of blood at $Q_{Bin} = 200$ mL/min, $Q_{Din} = 500$ mL/min.
[a]Clearance enhancement $= (C_L - C_{Lo})/C_{Lo}$ where C_L and C_{Lo} are the clearances measured at any ultrafiltration rate different from zero and at zero ultrafiltration rate, respectively.
SSR sum of squared residuals.

TABLE 5. Comparison of experimental data[16] with the predictions obtained from Legallais *et al.*'s model[20] and the model in this article for the enhancement of Vitamin B12 clearance.

Q_F (mL/min)	Clearance enhancement[a] Experimental	Legallais *et al.*[20]	This article
20	0.134	0.137	0.135
40	0.235	0.241	0.241
60	0.413	0.411	0.415
SSR		4.90×10^{-5}	4.10×10^{-5}

Data were collected using saline in substitution of blood at $Q_{Bin} = 200$ mL/min, $Q_{Din} = 500$ mL/min.
[a]Clearance enhancement $= (C_L - C_{Lo})/C_{Lo}$ where C_L and C_{Lo} are the clearances measured at any ultrafiltration rate different from zero and at zero ultrafiltration rate, respectively.
SSR sum of squared residuals.

TABLE 6. Comparison of experimental data[16] with the predictions obtained from Legallais *et al.*'s model[20] and the model in this article for the enhancement of myoglobin clearance.

Q_F (mL/min)	Clearance enhancement[a] Experimental	Legallais *et al.*[20]	This article
20	0.350	0.450	0.463
40	0.930	1.015	0.982
60	1.740	1.695	1.713
SSR		1.93×10^{-2}	1.62×10^{-2}

Data were collected using saline in substitution of blood at $Q_{Bin} = 200$ mL/min, $Q_{Din} = 500$ mL/min.
[a]Clearance enhancement $= (C_L - C_{Lo})/C_{Lo}$ where C_L and C_{Lo} are the clearances measured at any ultrafiltration rate different from zero and at zero ultrafiltration rate, respectively.
SSR sum of squared residuals.

a priori to make the model predictive. For example, in the case of Hospal Filtral 12 AN69 dialyzer, the diffusive permeabilities of all the three solutes were unknown; therefore, they were obtained by minimizing the difference between the experimental and predicted clearance data. This fact simply limits the use of this model in evaluating the performance of new developed hemofilters.

We have also validated the model predictions with the experimental data reported by Bosch *et al.*[2] for Fresenius F60 type module. The structural properties of this module are listed in Table 7. Experimental data include the clearances of creatinine and inulin as well as the pressure drop through blood and dialysate sides measured at different ultrafiltration rates in both saline and plasma conditions. The results shown in Table 8 indicate that our predictions are within maximum 0.9 and 2.9% of the experimental value for creatinine and inulin, respectively. Considering the experimental error for each data point, it can be concluded that model predictions are in good agreement with the data collected for both ultrafiltration rates. Bosch *et al.*'s data are the only data available in the literature which can be used to investigate the influence of protein adsorption on the removal rate of solutes. Both model predictions and experimental data indicate that protein adsorption has no influence on the clearance of creatinine, while inulin clearance from plasma is slightly lower at zero net ultrafiltration rate, and identical in both medium at the ultrafiltration rate of 50 mL/min. The comparison of predictive ability of our model with that of Legallais *et al.*'s model is shown in Fig. 4. Clearly, our model yields more accurate predictions especially for the clearance enhancement of inulin. This is due to the fact that in the model of Legallais *et al.*[20] protein adsorption on the membrane surface is neglected. We expect that the influence of protein adsorption on the whole body clearances of larger molecular weight solutes such as myoglobin would be more pronounced. Bosch *et al.*[2] have also measured inlet and outlet pressures in the dialysate and blood compartments of the Fresenius F60 type module using electrolyte and plasma solutions in substitution of blood. These pressure values at each net ultrafiltration rate were also predicted by our model. The results in Figs. 5 and 6 show that model predictions are in good agreement with the experimental data. Most of the deviations in predicted values were found to be in the range of 1–10%, and the maximum deviation was around 25%.

The Comparison of Predictive Ability of Full Model and Simplified Models

As shown in the theory section, the model developed in this study takes into account simultaneous mass and momentum transfers not only in the axial but also in the radial direction. In addition, the adsorption of large molecular weight proteins (MW > 60,000 Da) on

TABLE 7. Structural properties of the F60 type hemodialyzer.[20]

	Effective length (cm)	Fiber radius (μm)	Number of fibers	Inner housing diameter (cm)	Thickness (μm)
Fresenius 60 type hemodialyzer	22	200	9000	4.0	40

	Membrane area (m^2)	Porosity	Pore size (Å)	Fraction of dense layer	Hydraulic permeability (cm/s mmHg)
Fresenius 60 type hemodialyzer	1.25	0.8	7.9	0.0217	3.36×10^{-6}

TABLE 8. Comparison of experimental data[2] with the predictions obtained from the model in this article for creatinine and inulin clearances.

	Clearance (mL/min)		Clearance (mL/min)	
	Experiment[2]		Model in this article	
Q_{UF} (mL/min)	Creatinine	Inulin	Creatinine	Inulin
Saline				
0	173.3 ± 2.5	95.6 ± 4.1	174.5	96.7
50	183.4 ± 2.7	117.2 ± 4.9	184.2	120.4
Plasma				
0	172.2 ± 2.8	91.3 ± 8.4	173.7	93.9
50	183.4 ± 4.0	18.9 ± 3.4	184.0	120.0

Data were collected using F60 type hemodialyzer where Q_{Bin} = 200 mL/min, Q_{Din} = 500 mL/min.

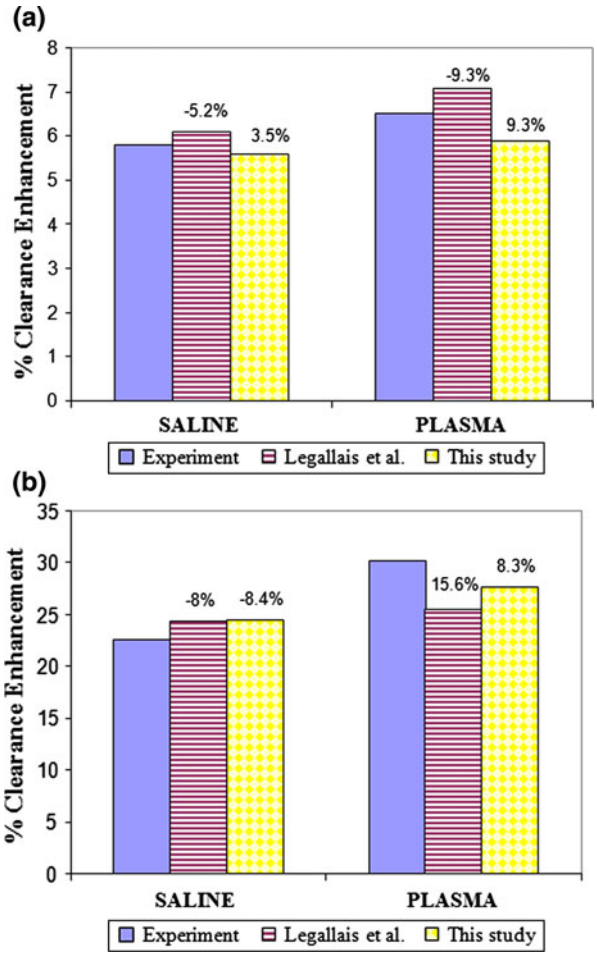

FIGURE 4. Comparison of experimental data[2] with the predictions obtained from Legallais *et al.*'s model[20] and the model in this article for the enhancement of (a) creatinine, (b) inulin clearances. Data were collected at Q_{Bin} = 200 mL/min, Q_{Din} = 500 mL/min, and clearance enhancement is calculated based on difference in the clearances measured at the net ultrafiltration rates of 0 and 50 mL/min. Numbers on the bars represent % relative error in predicting the experimental data.

the inner surface of the membrane is also considered. To illustrate the importance of including the radial concentration gradients and protein adsorption kinetics in the model, the experimental data used in the previous section were also predicted without considering these effects. The results obtained from full and simplified models by neglecting the radial concentration gradient and the protein adsorption are shown in Tables 9, 10, 11, and 12. From these results, it is obvious that neglecting radial concentration gradient leads to higher error in predicting the experimental data. In Table 12, although considering the protein adsorption on the inner surface of the membrane gives closer predictions to the experimental mean values, both simplified and full model estimations are statistically in good agreement with the experimental data.

Model Predictions

According to the model derived in this study, the performance of the hemodialyzer is influenced by the flow characteristics on the blood and dialysate sides, protein adsorption kinetics, structural properties of the membrane, and the design of the module. The model predictions can provide axial and radial velocity profiles through the blood side, the change in the thickness of the adsorbed protein layer, as well as the solute and pressure profiles through the blood and dialysate sides. Some of the output results from the model are illustrated in Figs. 7, 8, 9, 10, 11, and 12 obtained for dialysis through Fresenius 60 (F60) type hemodiafilter

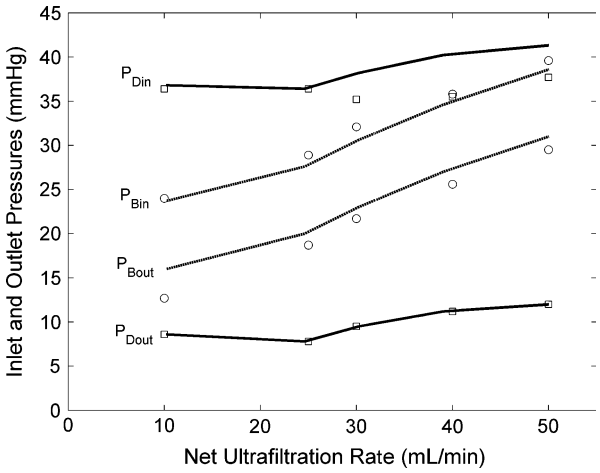

FIGURE 5. Comparison of predicted inlet and outlet pressures of blood and dialysate compartments with the experimental data[2] measured using saline solution in substitution of blood.

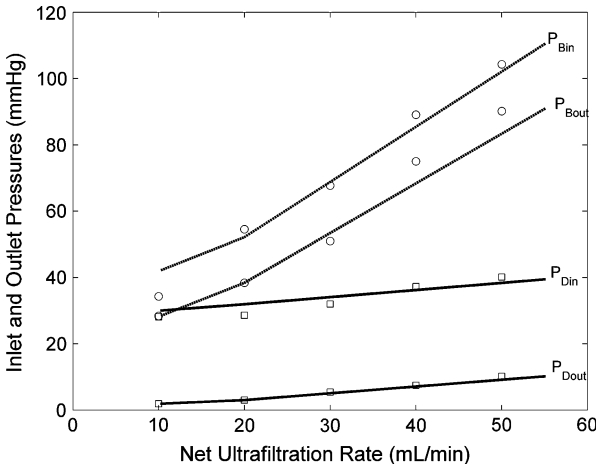

FIGURE 6. Comparison of predicted inlet and outlet pressures of blood and dialysate compartments with the experimental data[2] measured using plasma in substitution of blood.

TABLE 9. Comparison of experimental data[16] with the predictions obtained by uniform and nonuniform radial concentrations in the model for the enhancement of creatinine clearance.

		Clearance enhancement[a]	
Q_F (mL/min)	Experimental	Nonuniform radial concentration	Uniform radial concentration
20	0.0513	0.0531	0.0930
40	0.1245	0.1069	0.1780
60	0.1866	0.1583	0.2451
SSR		1.1×10^{-3}	8.0×10^{-3}

Data were collected using saline in substitution of blood at $Q_{Bin} = 200$ mL/min, $Q_{Din} = 500$ mL/min in the Hospal Filtral 12 AN69 dialyzer.
[a]Clearance enhancement $= (C_L - C_{Lo})/C_{Lo}$ where C_L and C_{Lo} are the clearances measured at any ultrafiltration rate different from zero and at zero ultrafiltration rate, respectively.
SSR sum of squared residuals.

TABLE 10. Comparison of experimental data[16] with the predictions obtained by uniform and nonuniform radial concentrations in the model for the enhancement of Vitamin B12 clearance.

		Clearance enhancement[a]	
Q_F (mL/min)	Experimental	Nonuniform radial concentration	Uniform radial concentration
20	0.134	0.135	0.146
40	0.235	0.241	0.258
60	0.413	0.415	0.421
SSR		4.81×10^{-5}	7.37×10^{-4}

Data were collected using saline in substitution of blood at $Q_{Bin} = 200$ mL/min, $Q_{Din} = 500$ mL/min in the Hospal Filtral 12 AN69 dialyzer.
[a]Clearance enhancement $= (C_L - C_{Lo})/C_{Lo}$ where C_L and C_{Lo} are the clearances measured at any ultrafiltration rate different from zero and at zero ultrafiltration rate, respectively.
SSR sum of squared residuals.

TABLE 11. Comparison of experimental data[16] with the predictions obtained by uniform and nonuniform radial concentrations in the model for the enhancement of myoglobin clearance.

		Clearance enhancement[a]	
Q_F (mL/min)	Experimental	Nonuniform radial concentration	Uniform radial concentration
20	0.350	0.463	0.510
40	0.930	0.982	1.144
60	1.740	1.713	1.921
SSR		1.62×10^{-2}	1.04×10^{-1}

Data were collected using saline in substitution of blood at $Q_{Bin} = 200$ mL/min, $Q_{Din} = 500$ mL/min in the Hospal Filtral 12 AN69 dialyzer.
[a]Clearance enhancement $= (C_L - C_{Lo})/C_{Lo}$ where C_L and C_{Lo} are the clearances measured at any ultrafiltration rate different from zero and at zero ultrafiltration rate, respectively.
SSR sum of squared residuals.

using input data listed in Tables 2 and 7. Simulations were performed at $t = 0$ allowing us to make a better assessment of the initial conditions on the solute clearances and the protein adsorption. As observed from Fig. 7 that at the beginning of the dialysis, urea concentration decreases dramatically along the length of the module, and this change becomes very small as the outlet of the fiber is approached. It should also be noted that solute concentration is the greatest at the center of the fiber and decreases significantly toward the membrane surface within the first half of the module. In the previous section, we have shown that the assumption of a uniform cross-sectional concentration profile can cause significant deviation in the predicted values from the experimental data. This result along with that shown in Fig. 7 simply indicates that the concentration gradient in the radial direction

TABLE 12. Comparison of experimental clearance data[2] with the predictions obtained by considering and neglecting protein adsorption in the model.

	Clearance (mL/min)		Clearance (mL/min)		Clearance (mL/min)	
	Experiment[2]		Full model[a]		Simplified model[b]	
Q_{UF} (mL/min)	Creatinine	Inulin	Creatinine	Inulin	Creatinine	Inulin
0	172.2 ± 2.8	91.3 ± 8.4	173.7	93.9	174.1	95.8
50	183.4 ± 4.0	118.9 ± 3.4	184.0	120.0	184.2	120.4
SSR			2.61	7.97	4.25	22.25

Data were collected using F60 type hemodialyzer where $Q_{Bin} = 200$ mL/min, $Q_{Din} = 500$ mL/min.
[a]The model takes into account protein adsorption on the inner surface of the membrane.
[b]The model neglects protein adsorption on the inner surface of the membrane.
SSR sum of squared residuals.

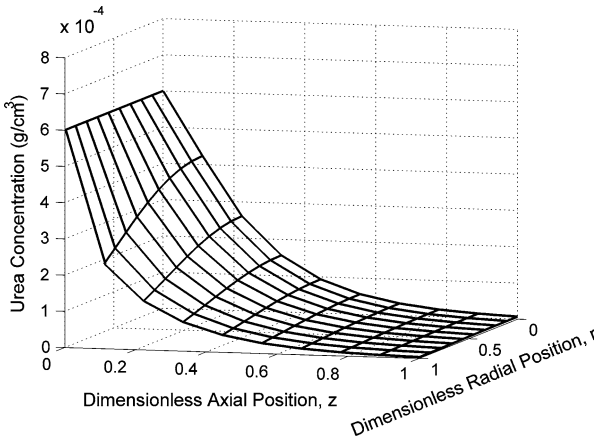

FIGURE 7. The change of urea concentration in axial and radial directions.

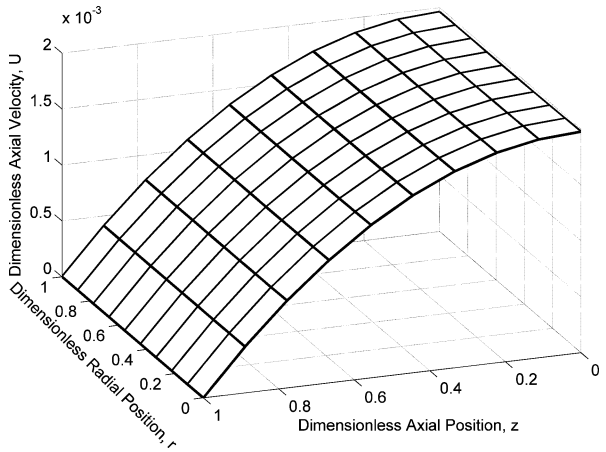

FIGURE 8. The change of axial velocity in axial and radial directions.

plays an important role on mass transfer during hemodialysis. In our model, convection is assumed to be the dominant mass transfer mechanism in the axial direction. Thus, the change in the axial velocity with respect to axial and radial directions is taken into account (Fig. 8). As expected, axial velocity is found to be at its maximum at the center and zero at the membrane surface. The concentration gradient of large blood molecules affects the viscosity of the blood, and this causes a change in axial velocity along the length of the fiber, smaller than the change with respect to radial position. The dimensionless radial velocity profiles through axial and radial directions are shown in Figs. 9a and 9b, respectively. It is worth emphasizing that the radial velocity is driven by the bulk flow of the fluid, which depends on the change of axial velocity in z-direction according to Eq. (3). Hence, total volumetric flux, J_v, which is developed by the local transmembrane pressure difference is an important factor on the magnitude of radial velocity by regulating the volumetric flow rate of blood at each position along the fiber length. It is observed that the radial velocity reaches a maximum at the inlet of the dialyzer and then starts decreasing along the fiber. This maximum is different for each radial position. Throughout the cross section, the radial velocity increases from the center to the membrane surface and the velocity gradient becomes smaller as the fiber outlet is approached. The solute transfer in the radial direction is carried out both by convection and diffusion mechanisms. Figure 10 shows the diffusive and convective fluxes of the rejected large protein molecules at different axial positions. Positive signs for the convective and net total flux of the protein imply that protein molecules are carried from the center of the fiber toward the membrane surface by convective mass transfer. Protein molecules rejected and not adsorbed by the membrane surface, diffuse back to the center of the fiber by diffusion, and therefore, diffusive flux becomes negative. The results shown in Figs. 9 and 10 clearly indicate the importance of the radial velocity profile especially in the radial direction which directly influences the rate of protein transfer and, consequently, the rate of protein adsorption on the surface of the membrane. As illustrated in Fig. 11, protein adsorption takes place

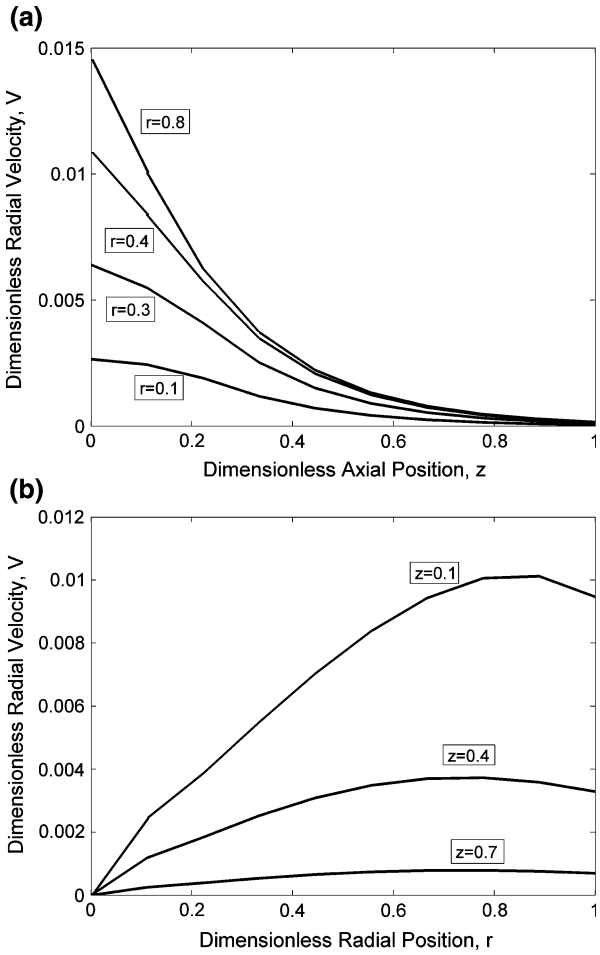

FIGURE 9. The change of radial velocity along (a) the length of fiber and (b) in cross section.

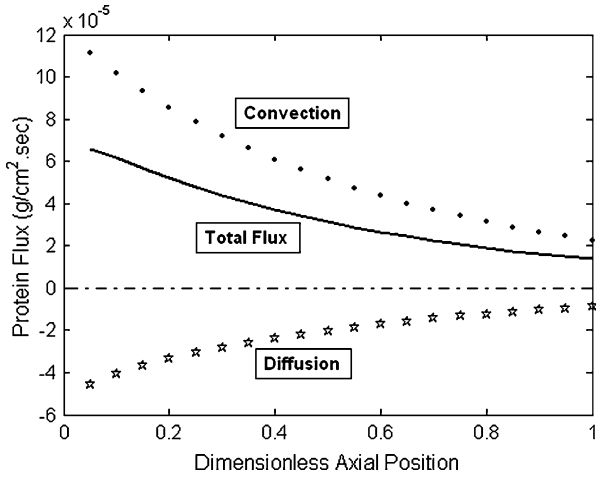

FIGURE 10. The change of protein flux with respect to axial position.

quickly at the beginning of the dialysis as equilibrium is reached within almost half an hour. The change in the protein layer thickness in the axial direction is

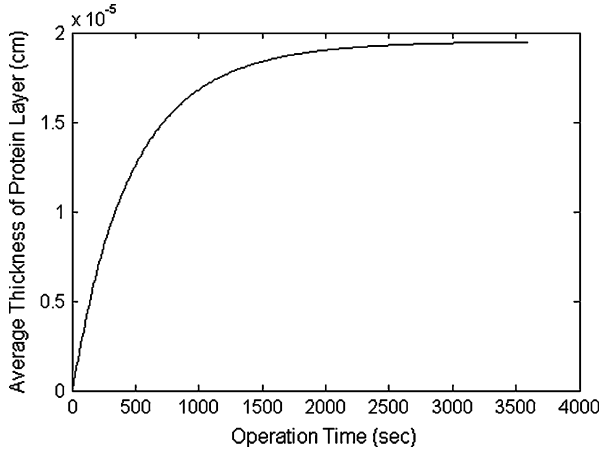

FIGURE 11. The change of adsorbed protein layer thickness with respect to time.

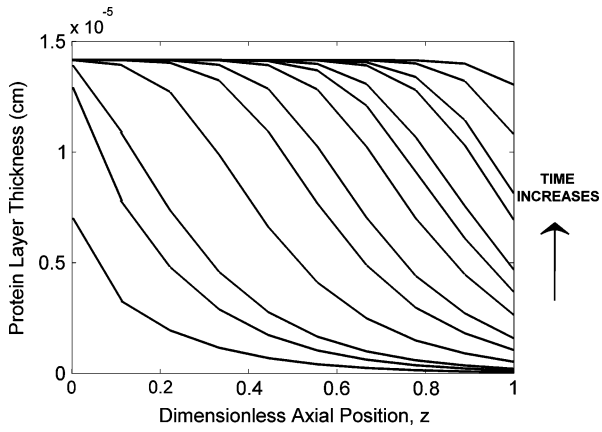

FIGURE 12. The change of protein layer thickness along the fiber length at different times.

shown in Fig. 12 at multiple time points during 1 h of hemodialysis operation. It is observed that, at the initial stages of the operation, the thickness of the protein layer decreases as the dialyzer outlet is approached which is caused by lower convectional protein transport toward the membrane surface. On the other hand, as the operation time increases, the difference in protein layer thickness between the inlet and outlet of the dialyzer becomes smaller until uniform thickness is achieved when equilibrium protein adsorption capacity of the surface is reached.

Whole Body Clearances

Clinically, the effectiveness of the hemodialysis operation is evaluated by checking the solute concentration levels in patient's blood. Theoretically, the solute concentrations in patient's blood can be calculated by combining the dialyzer and intercompartmental clearances (Fig. 1). In this section, the effects of

membrane structural parameters, operating conditions, and dimensions of the dialyzer on the removal of model solutes from patient's blood were investigated, and the results are listed in Table 13. A reference set of parameters was chosen based on the typical values available for commercial dialyzers, and each parameter was altered within a reasonable range that was selected from the clinical studies reported in the literature. Urea, vitamin B12, and inulin were chosen as model solutes with three different molecular weights, and the % removal of these solutes was calculated using their initial and final concentrations in blood at the end of a typical dialysis time of 4 h. Model calculations show that increasing the blood and dialysate flowrates has a significant influence on the clearance of urea, and this effect decreases with the increasing solute size suggesting that the clearance of urea is controlled by the conditions on the blood and dialysate sides. Although *Sh* number and, therefore, the dialysate side mass transfer coefficient increase with dialysate flowrate according to the Eq. (37), it does not significantly affect the removal of large solutes such as inulin, since the mass transfer of large solutes is controlled by the membrane resistance. Thus, the removal of the large solutes is more likely influenced by the changes in the structural properties of the membrane. Solute removal rates decrease with the increases in total thickness of the membrane and the fraction of dense skin layer, while enhancements in the removal of all solutes are observed with the increases in porosity and pore size of the membrane. The clearances of larger solutes are more influenced by variations in the structural parameters of the membrane since overall mass transfer resistance of large solutes is mainly controlled by their transport through the membrane. The increases in fiber length and fiber radius improve the rate of removal of all solutes from blood due to longer residence time of the blood in the dialyzer. Noda and Gryte[28] found that the overall mass transfer coefficient is not only a function of the membrane thickness, membrane type, and nature of the solute but it is also influenced by the packing density of the hollow fibers in the dialyzer shell. Their calculations show that there is an optimal packing density of the fibers. Very tightly packed hollow fiber dialyzers do not always lead to efficient mass transfer due to a decrease in available membrane surface area. Our results shown in Table 13 are in agreement with their calculations in that the increasing the distance between the fibers by increasing the inner housing diameter of the dialyzer, d_{housing}, enhances the removal of all solutes from blood. Varying the inner housing diameter was found to be much more effective than that of the fiber radius for increasing the efficiency of the hemodialysis operation.

TABLE 13. The effects of different model parameters on percent removal of solutes from the blood.

	Solutes		
Parameters	Urea	Vitamin B12	Inulin
Q_B (mL/min)			
100	52.61	38.97	9.51
200	69.40	44.48	10.75
300 (R)	75.07	46.57	11.03
Q_D (mL/min)			
300	63.37	36.21	8.57
400	66.56	40.15	9.59
500 (R)	69.40	44.48	10.75
Thickness (μm)			
20	70.51	49.95	16.28
46 (R)	69.40	44.48	10.75
60	68.79	41.94	9.02
Porosity			
0.3	65.97	33.20	5.15
0.5	68.18	39.71	7.83
0.8 (R)	69.40	44.48	10.75
Pore size (Å)			
8	69.13	37.57	2.55
13	69.23	42.35	5.54
18 (R)	69.40	44.48	10.75
Fraction of dense layer			
0	70.12	53.67	21.71
0.02 (R)	69.40	44.48	10.75
0.1	69.38	43.98	6.11
R_i (μm)			
100	69.40	44.48	10.75
110 (R)	69.54	46.26	11.54
120	70.80	47.89	12.12
L (cm)			
10	59.44	29.01	5.57
20 (R)	69.40	44.48	10.75
30	72.47	53.68	12.09
d_{housing} (cm)			
2.5	48.02	22.75	5.25
3.9 (R)	69.40	44.48	10.75
4.8	71.36	48.14	13.62

% Removal of solute $= \frac{(\rho_i^B|_{t=0} - \rho_i^B|_{t=4\,h})}{\rho_i^B|_{t=0}} \times 100$.

(R) denotes "Reference Case," and all other parameters used in simulations are listed in Table 2.

We have also utilized whole body clearance model to investigate the influence of protein adsorption on the dialysis time of the solutes. In the previous section, it was shown that with the inclusion of protein adsorption, our model yields more accurate prediction of the clearance data collected using plasma in substitution of blood. Based on this confirmation, it is reasonable to expect that hemodialysis time should be predicted more accurately with the inclusion of the protein adsorption kinetics in the mathematical model. Figure 13 shows that neglecting protein adsorption on the inner surface of the membrane leads to prediction of shorter treatment time of approximately 20 min to remove 95% of inulin initially present in blood. It is expected that this

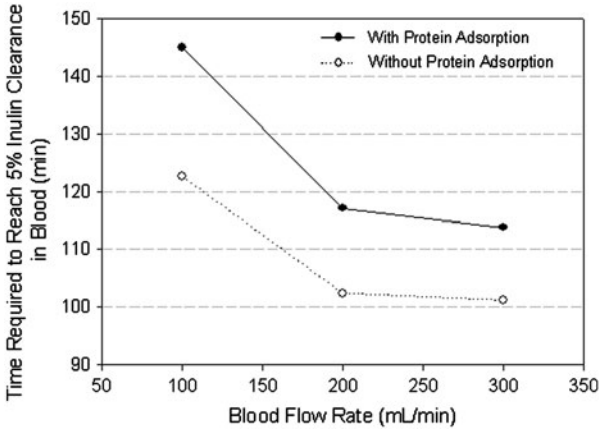

FIGURE 13. Time required to remove 95% of inulin initially present in blood at different blood flow rates. Simulations were performed for two cases; (○) without protein fouling, (●) with protein fouling.

difference in the predicted dialysis times due to the effect of protein adsorption will be even greater for the clearance of larger molecular weight solutes. This simply proves once more the importance of inclusion of the protein adsorption in the model.

CONCLUSION

In this study, we have developed a mathematical model which can be used to predict the *in vitro* performance of commercial hemodialysis units. Both axial and radial variations in the velocity and concentrations in the blood compartment were taken into account along with the adsorption of rejected, large protein molecules on the inner surface of the membrane. The results have clearly shown that neglect of radial concentration gradient leads to higher error in predicting the experimental data. The model predictions both with and without consideration of the protein adsorption on the inner surface of the membrane were statistically in good agreement with the experimental data, although the model considering protein adsorption gave closer values to the experimental means. In addition, shorter dialysis time was predicted without considering protein adsorption which may cause misleading conclusions in evaluating the performance of the hemodialysis unit. The model does not include any fitting parameter, and its predictions were found to be in good agreement with the available experimental data. Thus, it is fair to conclude that the model can be used as a tool either by clinicians to investigate the influences of blood and dialysate flowrates or by researchers to optimize module design and structure of the membrane.

To our knowledge, this is the first study which takes into account not only simultaneous mass and momentum transfers on the blood side both in radial and axial directions, but also the accumulation of rejected large molecules on the surface of the membrane. Obviously, this model is a first step toward an accurate description of solute transport and protein adsorption. In the future, the model could be further extended to consider the internal fouling phenomena caused by adsorption of middle molecular weight proteins on the pore walls and the change in hydraulic permeability associated with both internal and external fouling.

REFERENCES

[1]Abaci, H. E. Modeling of Hemodialysis Operation. MSc Thesis, Izmir Institute of Technology, 2008, pp. 48–50.
[2]Bosch, T., B. Schmidt, W. Samtleben, and H. J. Gurland. Effect of protein adsorption on diffusive and convective transport through polysulfone membranes. *Contrib. Nephrol.* 46:14–22, 1985.
[3]Bungay, P. M., and H. Brenner. The motion of a closely fitting sphere in a fluid filled tube. *Int. J. Multiphase Flow* 1:25–56, 1973.
[4]Cantor, R. C., and P. R. Schimmel. Biophysical Chemistry. Part II—Techniques for the Study of Biological Structure and Function. New York: W.H. Freeman and Company, 1980.
[5]Chang, Y. L., and C. J. Lee. Solute transport characteristics in hemodiafiltration. *J. Membr. Sci.* 39:99–111, 1988.
[6]Clark, W. R., J. K. Leypoldt, L. W. Henderson, B. A. Mueller, M. K. Scott, and E. F. Vonesh. Quantifying the effect of changes in the hemodialysis prescription on effective solute removal with a mathematical model. *J. Am. Soc. Nephrol.* 10:601–609, 1999.
[7]Dahuron, L., and E. L. Cussler. Protein extraction with hollow fibres. *AIChE J.* 34(1):130–136, 1988.
[8]Deen, W. M. Hindered transport of large molecules in liquidfilled pores. *AIChE J.* 33:1409, 1987.
[9]Eloot, S. Experimental and Numerical Modeling of Dialysis. Doctorate Thesis. Ghent University, 2005.
[10]Gachon, A. M. F., J. Mallet, A. Tridon, and P. Deteix. Analysis of proteins eluted from hemodialysis membranes. *J. Biomater. Sci. Polym.* 2:263–276, 1991.
[11]Gast, K., H. Damaschun, R. Misselwitz, M. M. Frohne, D. Zirwer, and G. Damaschun. Compactness of protein molten globules: temperature-induced structural changes of the apomyoglobin folding intermediate. *Eur. Biophys. J.* 23:297, 1994.
[12]Giddings, J. C., E. Kucera, C. P. Russell, and M. N. Myers. Statistical theory for the equilibrium distribution of rigid molecules in inert porous networks: exclusion chromatography. *J. Phys. Chem.* 72:4397–4408, 1968.
[13]Hosoya, N., and K. Sakai. Backdiffusion rather than backfiltration enhances endotoxin transport through highly permeable dialysis membranes. *Trans. ASAIO* 36:311–313, 1990.
[14]Imholz, A. L. T., O. C. M. Koomen, D. O. Struijk, L. Arisz, and R. T. Krediet. Effect of increased intraperitoneal pressure on fluid and solute transport during CAPD. *Kidney Int.* 44:1078–1085, 1993.
[15]Incropera, F. P., and D. P. DeWitt. Fundamentals of Heat and Mass Transfer. New York: Wiley, 2002.

[16]Jaffrin, M. Y., L. H. Ding, and J. M. Laurent. Simultaneous convective and diffusive mass transfer in a hemodialyser. *J. Biomech. Eng*. 112:212–219, 1990.
[17]Kunimoto, T., E. G. Lowrie, and S. Kumazawa. Controlled ultrafiltration (UF) with hemodialysis (HD): analysis of coupling between convective and diffusive mass transfer in a new HD-UF system. *Trans. ASAIO* 23:234–243, 1977.
[18]Landis, E. M., and J. R. Pappenheimer. Handbook of Physiology—Circulation. Washington, DC: American Physical Society, p. 961, 1963.
[19]Langlois, W. E. Slow Viscous Flow. New York: McMillan, pp. 201–221, 1964.
[20]Legallais, C., G. Catapano, B. V. Harten, and U. Baurmeister. A theoretical model to predict the in vitro performance of hemodiafilters. *J. Membr. Sci*. 168:3–15, 2000.
[21]Leypoldt, J. K., A. K. Cheung, L. Y. Agodoa, J. T. Daugirdas, T. Greene, and P. R. Keshaviah. Hemodialyzer mass transfer-area coefficients for urea increase at high dialysate flowrates. *Kidney Int*. 51:2013–2017, 1997.
[22]Marconi, U. M. B., A. Puglisi, L. Rondoni, and A. Vulpiani. Fluctuation-dissipation: response theory in statistical physics. *Phys. Rep*. 461:111, 2008.
[23]Martinoli, R., E. I. Mohamed, C. Maiolo, R. Cianci, F. Denoth, S. Salvadori, and L. Iacopino. Total body water estimation using bioelectrical impedance: a meta-analysis of the data available in the literature. *Acta Diabetol*. 40:203–206, 2003.
[24]Morrette, R. A., and C. G. Gogos. Viscous dissipation in capillary flow of rigid PVC and PVC degradation. *Polym. Eng. Sci*. 8:272–280, 1968.
[25]Morti, S., J. Shao, and A. L. Zydney. Importance of asymmetric structure in determining mass transport characteristics of hollow fiber hemodialyzers. *J. Membr. Sci*. 224:39–49, 2003.
[26]Moussy, Y. Bioartificial kidney. I. Theoretical analysis of convective flow in hollow fiber modules: application to a bioartificial hemofilter. *Biotechnol. Bioeng*. 68:142–152, 2000.
[27]Nakamura, K., and K. Matsumoto. Properties of protein adsorption onto pore surface during microfiltration: effects of solution environment and membrane hydrophobicity. *J. Membr. Sci*. 280:363–374, 2006.
[28]Noda, I., and C. C. Gryte. Mass transfer in regular arrays of hollow fibers in countercurrent dialysis. *AIChE J*. 25(1):113–122, 1979.
[29]Pallone, T. L., and J. Petersen. A mathematical model of continuous arteriovenous hemofiltration predicts performance. *Trans. ASAIO* 33:304–308, 1987.
[30]Raff, M., M. Welsch, H. Göhl, H. Hildwein, M. Storr, and B. Wittner. Advanced modeling of highflux hemodialysis. *J. Membr. Sci*. 216:1–11, 2003.
[31]Renkin, E. M. Filtration, diffusion, and molecular sieving through porous cellulose membranes. *J. Gen. Physiol*. 38(2):225–243, 1954.
[32]Sigdell, J. E. Calculation of combined diffusive and convective mass transfer. *Int. J. Artif. Organs* 5:361–372, 1982.
[33]Stiller, S., H. Mann, and H. Brunner. Backfiltration in hemodialysis with highly permeable membranes. *Contrib. Nephrol*. 46:23–32, 1985.
[34]Trusek-Holownia, A. A catalytic membrane for hydrolysis reaction carried out in the two-liquid phase system—membrane preparation and characterisation, mathematical model of the process. *J. Membr. Sci*. 259:74–84, 2005.
[35]Truskey, G. A., F. Yuan, and D. F. Katz. Transport Phenomena in Biological Systems. Upper Saddle River, NJ: Prentice Hall, p. 104, 2004.
[36]Werynski, A., and J. Wanieski. Theoretical description of mass transport in medical membrane devices. *Artif. Organs* 19(5):420–427, 1995.
[37]Wüpper, A., F. Dellanna, C. A. Baldamus, and D. Woermann. Local transport processes in high-flux hollow fiber dialyzers. *J. Membr. Sci*. 131:181–193, 1997.
[38]Wüpper, A., D. Woermann, F. Dellanna, and C. A. Baldamus. Retrofiltration rates in high-flux hollow fiber hemodialysers: analysis of clinical data. *J. Membr. Sci*. 121:109–116, 1996.